Chemical, Physical, and Mechanical Characterization of Isocyanate Cross-linked Amine-Modified Silica Aerogels

Atul Katti,[†] Nilesh Shimpi,[†] Samit Roy,*[,†] Hongbing Lu,*[,†] Eve F. Fabrizio,[‡] Amala Dass,[§] Lynn A. Capadona,[||] and Nicholas Leventis*[,||]

School of Mechanical and Aerospace Engineering, Oklahoma State University, Stillwater, Oklahoma 74078, Ohio Aerospace Institute, 22800 Cedar Point Road, Cleveland, Ohio 44142, Department of Chemistry, University of Missouri—Rolla, Rolla, Missouri 65409, and Materials Division-Polymers Branch, NASA Glenn Research Center, 21000 Brookpark Road, M.S. 49-1, Cleveland, Ohio 44135

Received June 26, 2005. Revised Manuscript Received October 24, 2005

We describe a new mechanically strong lightweight porous composite material obtained by encapsulating the skeletal framework of amine-modified silica aerogels with polyurea. The conformal polymer coating preserves the mesoporous structure of the underlying silica framework and the thermal conductivity remains low at 0.041 ± 0.001 W m^{-1} K^{-1}. The potential of the new cross-linked silica aerogels for load-carrying applications was determined through characterization of their mechanical behavior under compression, three-point bending, and dynamic mechanical analysis (DMA). A primary glass transition temperature of 130 °C was identified through DMA. At room temperature, results indicate a hyperfoam behavior where in compression cross-linked aerogels are linearly elastic under small strains (<4%) and then exhibit yield behavior (until 40% strain), followed by densification and inelastic hardening. At room temperature the compressive Young's modulus and the Poisson's ratio were determined to be 129 ± 8 MPa and 0.18, respectively, while the strain at ultimate failure is 77% and the average specific compressive stress at ultimate failure is 3.89×10^5 N m kg^{-1}. The specific flexural strength is 2.16×10^4 N m kg^{-1}. Effects on the compressive behavior of strain rate and low temperature were also evaluated.

1. Introduction

One of the most successful commercial uses of nanoparticles is as fillers in plastics.[1] For example, strength can be increased, and gas permeability can be lowered, by including a small weight percent (typically <5%) of an appropriate filler. As a result, significant efforts are being focused on improving the chemical compatibility between fillers and polymeric matrixes.[2] In this environment, we reasoned that if the amount of the filler and the polymer become comparable, then their roles can be reversed, so that if the filler, *or one of its forms*, has useful properties of its own, then those properties can be improved by "doping" with a polymer. The most common filler in use is silica, and a nanostructured form of silica, the silica aerogel, is a low-density, chemically inert material with low thermal conductivity, excellent acoustic insulation properties, and a highly interconnected porosity. With such properties, the silica aerogel can comprise the host of functional guests for use in air/water purification, catalysis, energy storage, and sensing,[3] rendering aerogels ideal materials for aerospace applications. However, aerogels have one serious drawback that has prevented not only their aerospace use but also their wider industrial and commercial use: aerogels are fragile materials. Thus far, they have found only very limited use as Cerenkov radiation detectors in certain types of nuclear reactors, in NASA's Stardust program for capturing hypervelocity particles in space, and as ultralightweight thermal insulators aboard planetary vehicles on Mars such as the Sojourner Rover in 1997 and the Spirit and Opportunity in 2004. Meanwhile, it is clear at this point that, from a materials perspective, all future space exploration (returning to the Moon and going to Mars) will rely decisively on weight reduction and multifunction. Therefore, if the excellent thermal insulating properties of aerogels could be combined with improved mechanical strength, aerogels will be ideal dual-function materials for this endeavor.

The aerogel fragility is ultimately traced to their structure. Nanoscopically, silica aerogels prepared through a base-catalyzed sol−gel route consist of a "pearl-necklace"-like fractal network of secondary silica nanoparticles with densities about half of that of dense silica.[3b] The large void space between those chains of particles is responsible for the low

* Corresponding authors: Tel.: 205-348-5883 (S. Roy); 405-744-5900 (H. Lu); 216-433-3202 (N. Leventis). E-mail: sroy@eng.ua.edu (S. Roy); hongbin@ceat.okstate.edu (H. Lu); Nicholas.Leventis@nasa.gov (N. Leventis).
[†] Oklahoma State University.
[‡] Ohio Aerospace Institute.
[§] University of Missouri—Rolla.
[||] NASA Glenn Research Center.

(1) Thayer, A. M. *Chem. Eng. News* **2003**, (Sept 1), 15.
(2) (a) Chen, Y.; Iroh, J. O. *Chem. Mater.* **1999**, *11*, 1218−1222. (b) Ahmad, Z.; Mark, J. E. *Chem. Mater.* **2001**, *13*, 3320−3330. (c) Campbell, S.; Scheiman, D. *High Perform. Polym.* **2002**, *14*, 17−30. (d) Mitchell, C. A.; Bahr, J. L.; Arepalli, S.; Tour, J. M.; Krishnamoorti, R. *Macromolecules* **2002**, *35*, 8825−8830.
(3) (a) Rolison, D. *Science* **2003**, *299*, 1698−1701. (b) Pierre, A. C.; Pajonk, G. M. *Chem. Rev.* **2002**, *102*, 4243−4265. (c) Morris, C. A.; Anderson, M. L.; Stroud, R. M.; Merzbacher, C. I.; Rolison, D. R. *Science* **1999**, *284*, 622. (d) Hüsing, N.; Schubert, U. *Angew. Chem., Int. Ed.* **1998**, *37*, 22−45.

10.1021/cm0513841 CCC: $33.50
Published on Web 12/16/2005

bulk density of aerogels. The fragility of the aerogel framework is traced to the interparticle connecting zones, referred to as necks. Necks are formed by coagulation of particles upon gelation and grow to a certain point by dissolution and reprecipitation of silica during aging of freshly made gels.[4] Consequently, it seemed reasonable that when the interparticle necks are rendered wider, the specific stiffness and strength of monolithic silica aerogels could be improved without incurring a severe weight penalty. That was first achieved by utilizing the naturally occurring hydroxyl functionality on the surfaces of the nanoparticles as the template for the conformal accumulation and polymerization of diisocyanates.[5] Thus, it was shown that the resulting aerogels could be up to 3 times more dense than aerogels based on the underlying silica framework, but up to 300 times stronger in terms of the force it takes to break them in a three-point bending test configuration. However, it was also discovered that the polymer accumulated on the surface of the nanoparticles is not polyurethane throughout.[5d] Diisocyanate reacts with the surface −OH groups on silica and attaches through carbamate (urethane) groups (−Si−O−CO−NH−) onto the silica nanoparticles, as designed. However, the interparticle tethers consist of polyurea, which is formed in two steps: first, via reaction of the dangling isocyanate groups with water used for gelation and remaining strongly adsorbed on the surface of the nanoparticles, and second, via reaction of the resulting amines dangling from the nanoparticle surfaces with more diisocyanate from the solution filling the mesopores.

Since cross-linking is mostly polyurea-based, and given that (a) the reaction of isocyanates with amines is generally faster than their reaction with hydroxyls[6] and (b) the resulting polyureas are generally stronger polymers than polyurethanes,[7] control of polyurea formation throughout the cross-linking process may produce even more robust aerogels. That will require surface modification of the skeletal silica nanopartices with amines. In turn, that has been achieved by co-gelation of tetramethoxysilane (TMOS) and 3-aminopropyltriethoxylsilane (APTES),[3d,8] and the resulting gels have been cross-linked successfully with epoxides and polystyrene through rather long and elaborate processes.[9] In this report, we combine amine-functionalized silica with isocyanate chemistry to produce, through a simplified process, mostly clear highly porous cross-linked silica aerogels with exceptional mechanical properties, which have been characterized through compressive and flexural bending tests. Thus, the specific compressive stress at ultimate failure is 3.89×10^5 N m kg^{-1}, while the thermal conductivity remains low, between the literature values reported for glass wool and Styrofoam. The effect of applied stress on the microporous structure is reported as a function of deformation by scanning electron microscopy (SEM) and surface area analysis by nitrogen adsorption.

2. Experimental Section

2.1. Materials. Acetonitrile, tetramethylorthosilicate (TMOS) and 3-aminopropyltriethoxysilane (APTES) were purchased from Aldrich and used as received. Desmodur N3200 hexamethylene diisocyanate oligomer was obtained courtesy of Bayer Corporation (Pittsburgh, PA). Deionized water was obtained from a Milli-Q water system purchased from Millipore, Inc. Liquid CO_2 (gas tank with siphon tube) used for supercritical fluid drying was obtained from AGA, Inc. (Cleveland, OH).

Wet gels by copolymerization of TMOS/APTES were prepared by essentially the same method published recently in conjunction with epoxy cross-linked aerogels.[9] In a typical procedure, two solutions, one containing 2.895 mL of TMOS, 0.965 mL of APTES, and 4.5 mL of CH_3CN (solution A) and another one containing 4.5 mL of CH_3CN and 1.5 mL of water (solution B) were cooled in a dry ice/acetone bath and mixed rapidly by adding solution B into solution A. The resulting sol was shaken vigorously and divided into appropriate molds. We employed 19.6 mm diameter, 20 cm^3 polyethylene syringes as the cylindrical molds for compression testing, and for the square cross-section samples used in the three-point bending testing we used 12.7 mm × 12.7 mm square cross-section plastic tubes. Molds with an 8 mm × 3 mm rectangular cross section for Dynamic Mechanical Analysis were custom-made by Ace Glass Inc. (Vineland, NJ). Square and rectangular cross-section molds were open at both ends; one end was covered with two layers of Parafilm, and the sol was poured from the other end, which was then also covered with two layers of Parafilm. Gelation takes place once the temperature reaches about room temperature (<1 min). Gels were allowed to stand (age) for 2 h and subsequently were removed from their molds and placed in fresh CH_3CN. Square and rectangular cross-section samples were pushed out of the molds using plastic plungers of the same cross-sectional shape and area as the internal cross section of the molds. The wash solvent-to-gel volume ratio was approximately 5:1. The solvent (CH_3CN) surrounding the gel was changed every day for 3 days at ∼24 h intervals.[10] Subsequently, the gels were placed in an isocyanate solution containing 32 g of Desmodur N3200 in 80 mL of CH_3CN and were allowed to equilibrate for 24 h under frequent agitation. At the end of the period, samples were removed from the isocyanate solution, placed in a new container with fresh CH_3CN, and heated in a 70 °C oven for 3 days. Next, the containers were cooled to room temperature and the gels were removed and placed in fresh CH_3CN, which was changed another three times in 24 h intervals. Finally, the gels were transferred in an autoclave equipped with a 1 L, 3 in. diameter pressure vessel (Applied Separations Model Spe-edSFE) filled with CH_3CN and extracted with liquid CO_2, which was taken out supercritically.

(4) Hæreid, S.; Anderson, J.; Einarsrud, M.-A.; Hua, D. W.; Smith, D. M. *J. Non-Cryst. Solids* **1995**, *185*, 221.
(5) (a) Leventis, N.; Sotiriou-Leventis, C.; Zhang, G.; Rawashdeh, A.-M. M. *Nano Lett.* **2002**, *2*, 957−960. (b) Zhang, G.; Rawashdeh, A.-M. M.; Sotiriou-Leventis, C.; Leventis, N. *Polym. Prepr.* **2003**, *44*, 35−36. (c) Bertino, M. F.; Hund, J. F.; Zhang, G.; Sotiriou-Leventis, C.; Tokuhiro, A. T.; Leventis, N. *J. Sol-Gel Sci. Technol.* **2004**, *30*, 43−48. (d) Zhang, G.; Dass, A.; Rawashdeh, A.-M. M.; Thomas, J.; Counsil, J. A.; Sotiriou-Leventis, C.; Fabrizio, E. F.; Ilhan, F.; Vassilaras, P.; Scheiman, D. A.; McCorkle, L.; Palczer, A.; Johnston, J. C.; Meador, M. A. B.; Leventis, N. *J. Non-Cryst. Solids* **2004**, *350*, 152−164. (e) Leventis, N.; Palczer, A.; McCorkle, L.; Zhang, G.; Sotiriou-Leventis, C. *J. Sol-Gel Sci. Technol.* **2005**, *35*, 99−105.
(6) (a) Wicks, Z. W., Jr.; Jones, F. N.; Pappas, S. P. *Organic Coatings Science and Technology Second Edition*; Wiley: New York, 1999; p 181. (b) Lu, Q.-W.; Hoye, T. R.; Macosko, C. W. *J. Polym. Sci., Part A: Polym. Chem.* **2002**, *40*, 23−10−2328. (c) Jackson, M. B.; Solomon, D. H. *J. Macromol. Sci., Chem.* **1972**, *6*, 671−687.
(7) See for example: Rosthauser, J. W.; Haider, K. W.; Steinlein, C.; Eisenbach, C. D. *J. Appl. Polym. Sci.* **1997**, *64*, 957−970.
(8) Hüsing, N.; Schubert, U.; Mezei, R.; Fratzl, P.; Riegel, B.; Kiefer, W.; Kohler, D.; Mader, W. *Chem. Mater.* **1999**, *11*, 451−457.
(9) Meador, M. A. B.; Fabrizio, E. F.; Ilhan, F.; Dass, A.; Zhang, G.; Vassilaras, P.; Johnston, J. C.; Leventis, N. *Chem. Mater.* **2005**, *17*, 1085−1098.
(10) Karl-Fisher analysis for water in the four successive CH_3CN wash baths gave 8672, 1262, 403, and 160 μg mL^{-1}, respectively. Fresh CH_3CN gave a water content equal to 60 μg mL^{-1}.

2.2. Chemical and Physical Characterization. Chemical and physical characterization was conducted by attenuated total reflectance (ATR) infrared and ^{13}C NMR spectroscopies, scanning electron microscopy (SEM), nitrogen adsorption porosimetry, He pycnometry, thermogravimetric analysis (TGA), and thermal conductivity analysis. ATR infrared spectra were obtained across the radius of disks cut from larger monoliths using a Nicolet Nexus 470 FT-IR spectrophotometer. For ^{13}C NMR spectroscopy, solid samples were ground by ball-milling for 5 min using a SPEX 5300 Mixer Mill (SPEX Inc., Edison, NJ) and spectra obtained on a Bruker Avance 300 Spectrometer, utilizing cross-polarization, magic angle spinning at 7 kHz, and spinning sideband suppression using a TOSS sequence. The spectra were externally referenced to the carbonyl of glycine (196.1 ppm relative to TMS). For SEM, samples were coated with Au and microscopy was conducted with an Hitachi S-4700 field emission microscope. For nitrogen adsorption porosimetry, samples were outgassed at 80 °C for 24 h and studies were conducted with an ASAP 2000 Surface Area/Pore Distribution analyzer (Micromeritics Instrument Corp.). TGA was performed using a TA Instruments Model 2950 HiRes instrument. Samples were run at a temperature ramp rate of 10 °C min^{-1} under nitrogen. Skeletal densities were determined with He pycnometry, using a Micromeritics AccuPyc 1330 instrument. Thermal conductivity was calculated from thermal diffusivity data collected with a Netzsch NanoFlash LFA 447 instrument employing a Xe flashlamp and a liquid N_2 cooled InSb sensor. Square samples (8 × 8 mm) for thermal diffusivity measurements were cut with a razor blade from ~1 mm thick disks, obtained by slicing as-prepared cylindrical monoliths with a diamond saw. The square samples were coated on both sides with a layer of vapor-deposited Au (~0.25 μm) and subsequently sprayed with a layer of Dry Graphite Film Lubricant (Miracle Power Products Corp., Cleveland, OH).

2.3. Dynamic Mechanical Analysis (DMA). The complex modulus was measured in a three-point bending mode on samples with nominal dimensions of 50 × 8 × 3 mm using a Dynamic Mechanical Analyzer Model RSA II (Rheometric Scientific Inc, Piscataway, NJ). Rectangular cross-sectional samples (see section 2.1) were supported by two knife edges on a forked fixture separated by a fulcrum span of 29.5 mm. A load was applied by a knife edge at the middle span of the bending specimen. The DMA test can thus be considered as a beam with pin−pin support loaded by a concentrated force applied in the middle of the beam. Temperature sweep DMA tests to determine glass transition temperatures were performed in the range between −132 and 210 °C. For this purpose, the use of a single fixed flexural frequency of 1 Hz was adequate. The fixture used in this type of test had a span of 29.5 mm, allowing for the specimen to shrink (as occurs at elevated temperatures) without separating from the fixture. The temperature sweep was started at −132 °C and the temperature was maintained at each successive neighboring value (until 210 °C) for 60 s. Sinusoidal (1 Hz) load and displacement data were acquired and processed at each temperature by the DMA apparatus.

2.4. Compression Testing. Compression testing was performed according to the ASTM D695-02a standard on cylindrical specimens, using a MTS machine (Model 810) equipped with a 55000 lb load cell. According to the ASTM standard, the height-to-diameter ratio of the specimen should be 2:1. Samples were cut using a 5200 rpm 10 in. compound power miter saw manufactured by Delta Machinery (Jackson, TN). The cut surfaces of the samples were polished using fine disk and belt grinders. Subsequently, powdered graphite lubricant (Panef Corporation, Milwaukee, WI) was sprayed on both the top and bottom faces of the specimen to reduce friction with the compression platens, and samples were placed between the top and bottom surfaces of a compression fixture. The top surface was held stationary whereas the bottom one was raised at a speed of 0.127 mm s^{-1} or higher, depending on the specified strain rate. The load was measured with a compression load cell, and the displacement data was directly acquired from the data acquisition software in conjunction with a LVDT (Linear Variable Differential Transformer). Compression tests were conducted at room temperature, as well as at lower temperatures: −27, −55, and −196 °C. For tests at −27 °C, samples were cooled in a freezer for 3 h. For tests at −55 °C, samples were placed inside a dewar (Model B, Precision Cryogenics Systems, Inc, Indianapolis, IN) with liquid nitrogen in the outer jacket for 3 h so that samples did not have direct contact with liquid nitrogen. The samples were then removed from the respective coolers and immediately tested in air within a span of 2 min. For testing at −196 °C the samples were directly immersed in liquid nitrogen for 30 min and immediately tested on the compression fixture at room temperature. Temperature of the specimen surface was measured by a thermocouple attached to the surface of the specimen. Due to the relatively small size of the specimen, it was assumed that the entire specimen reached thermal equilibrium over the time period allowed for the cool-down. The load-displacement curve for each test was converted to a stress−strain curve by dividing the load by the original cross-sectional area of the specimen (average cross-sectional area of the specimens was 230 mm^2) and the displacement by the height of the specimens (average height of the specimens was 33 mm). The compressive stress at ultimate failure, the strain at failure, and the Young's modulus were extracted from the stress−strain curves. The strain at failure was the strain at which the macroscopic failure of the specimen occurred. The influence of strain rate on compression of samples was quantified by comparing the stress−strain curves. Samples were loaded at strain rates of 0.0035, 0.035, and 0.35 per second.

2.5. Flexural Testing. The procedure for the three-point bending tests followed the ASTM standard D790. That standard, however, specifies a length/width ratio of 16. Such high-ratio samples are more difficult to make, mainly because of the difficulty in handling native wet gels before cross-linking. To circumvent this problem, we used nonstandard rectangular samples with nominal dimensions of ~11 × 11 × 50 mm. This gives a length/width ratio of 4.56, which is on the borderline between thin and thick beam testing. To determine the stress−strain relation, we corrected for the shear energy. Further details on the shear energy correction are given in section 3.2.c. The flexural experiments were conducted on an INSTRON Model 4202 (Instron Corporation, Norwood, MA) universal testing machine equipped with a 46 kg load cell and a Proportional, Integral, Derivative (PID) servo control. The crosshead speed was 2.54 mm min^{-1} and the fulcrum span was 50 mm. The load and displacement data were acquired using the NI LabView data acquisition software (National Instruments, Austin, TX). Flexural tests were conducted at room temperature (21 °C) and −196 °C. For the test at −196 °C the samples were directly immersed in liquid nitrogen for 10 min and immediately tested on the bending fixture at room temperature. As mentioned earlier, temperature of the specimen surface was measured by a thermocouple attached to the surface of the specimen.

3. Results and Discussion

3.1. Cross-linking Amine-Modified Silica Aerogels: Preparation and Characterization. Aerogels for this work were prepared by cross-linking an amine-modified silica framework produced by co-gelation of APTES and TMOS (Figure 1). The cross-linker was a hexamethylene diisocyanate oligomer supplied by Bayer Corporation Coatings

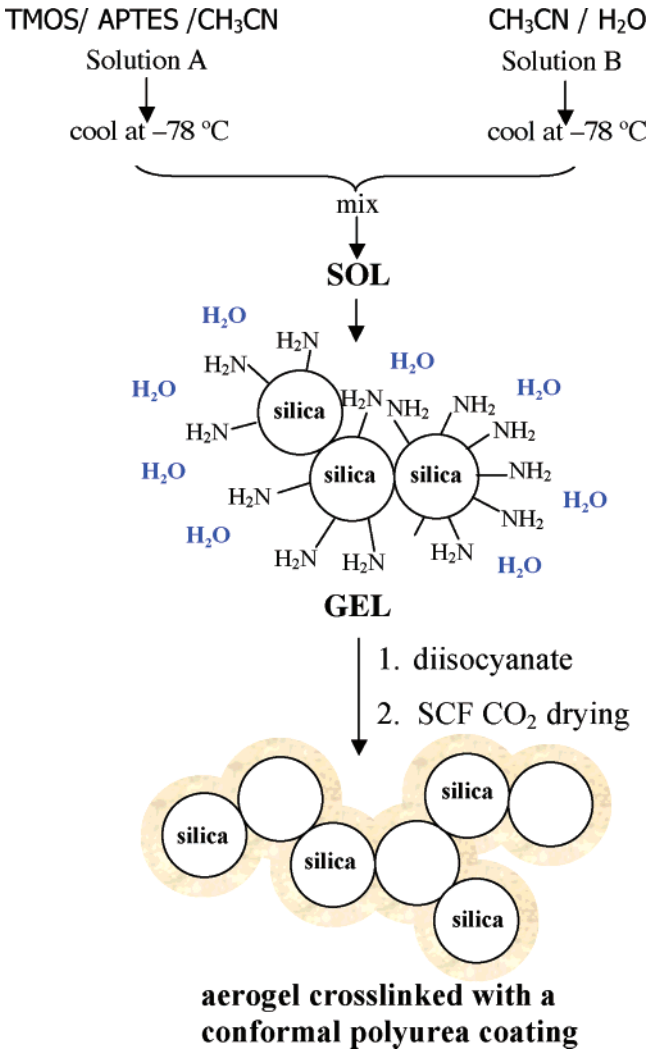

Figure 1. Preparation flowchart of polyurea cross-linked, amine-modified silica aerogels.

(Desmodur N3200). The exact conditions (Experimental Section) were chosen so that (a) native (non-cross-linked)

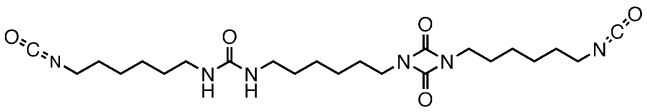

N3200 diisocyanate

aerogels would have approximately the same density as the non-amine-modified networks we have reported before[5] and (b) cross-linked aerogels would also have approximately the same density as our previous most dense isocyanate cross-linked non-amine-modified samples.[5] For this, our previously described procedure was modified by replacing one-fourth of the volume of TMOS with APTES. Thus, native APTES-modified aerogels of this study have a density of 0.190 ± 0.014 g cm^{-3} (versus 0.169 ± 004 g cm^{-3} of non-APTES-modified aerogels), while cross-linked APTES-modified aerogels have shrunk by about 14 ± 2% relative to the size of the molds, and the density of specimens used for all further characterization was 0.478 ± 0.004 g cm^{-3} (versus 0.447 ± 0.020 g cm^{-3} of the corresponding non-APTES-modified monoliths).[5a]

In the new modified procedure, APTES plays the dual role of the reagent and the (base) catalyst. Hence, owing to the high catalyst concentration, gelation at room temperature takes place almost instantaneously upon mixing the two sol precursors. To allow time for pouring the sol in the molds, the two sol precursors were cooled just prior to mixing in a dry ice/acetone bath. In that regard, cooling provides control over the gelation process, which will be important for large-scale production. Since hydrolysis of APTES is slower than hydrolysis of TMOS,[3d,8] APTES adds the amine functionality where it is needed the most for cross-linking, namely, at the surface of the skeletal nanoparticles.[3d,8,9] Furthermore, since amines react with isocyanate faster than hydroxyls,[6] cross-linking starts at room temperature. This renders wet gels easier to handle early in the process and facilitates fabrication of larger monoliths. Finally, isocyanate cross-linked wet gels were dried with supercritical CO_2. Currently, the largest monoliths we have prepared are ~3 in. in diameter, where the size is limited only by the size of our current autoclave. Typical monoliths are shown in Figure 2.

Like typical native silica aerogels, isocyanate-cross-linked amine-modified monoliths appear bluish in reflection. Most importantly, however, and in contrast to our previously reported isocyanate-cross-linked non-APTES-modified silica aerogels, the new material is colorless (as opposed to yellow) and translucent (as opposed to opaque). The absence of color is attributed to switching from a methanol/acetone to a new all-acetonitrile procedure: as previously discussed,[5d] in the course of cross-linking, isocyanate reacts with water adsorbed on silica and forms amines, which in turn react with more isocyanate from the solution filling the mesopores to form interparticle tethers. In the presence of acetone, amines may also react with the carbonyl group to form yellow imines. The translucency of cross-linked aerogels based on an APTES-modified silica backbone is attributed to their internal structure, which is shown in Figure 3B in comparison with the structure of native (non-cross-linked) APTES-modified silica aerogels (Figure 3A). Clearly, the polymer conformally coats the surface of the skeletal nanoparticles, leaving the mesoporous voids open. Meanwhile, the skeletal framework of APTES-modified aerogels appears to incorporate a larger number of particles than what we have observed previously with typical native silica aerogels.[5] Consistent with this observation, the BET surface area and the average pore diameter of Desmodur N3200 cross-linked APTES-modified silica aerogels are 261 m^2 g^{-1} and 9.7 nm, respectively, as opposed to 165 m^2 g^{-1} and 16.6 nm obtained with non-APTES-modified cross-linked aerogels of similar density. All data seem to suggest smaller particles in the case of amine-modified silica, and their formation is attributed to the high concentration of catalyst (APTES). Conformal coating of such particles with the isocyanate-derived polymer does not increase their size significantly, which apparently remains below the wavelength of light causing minimal scattering.

In addition to an all-acetonitrile process, a second innovation was in the cross-linking process itself: after incorporation of the isocyanate solution in the mesopores through room-temperature diffusion, gels were removed from the cross-linking solution and placed in *fresh solvent* (CH_3CN) before being heated at 70 °C to accelerate and complete

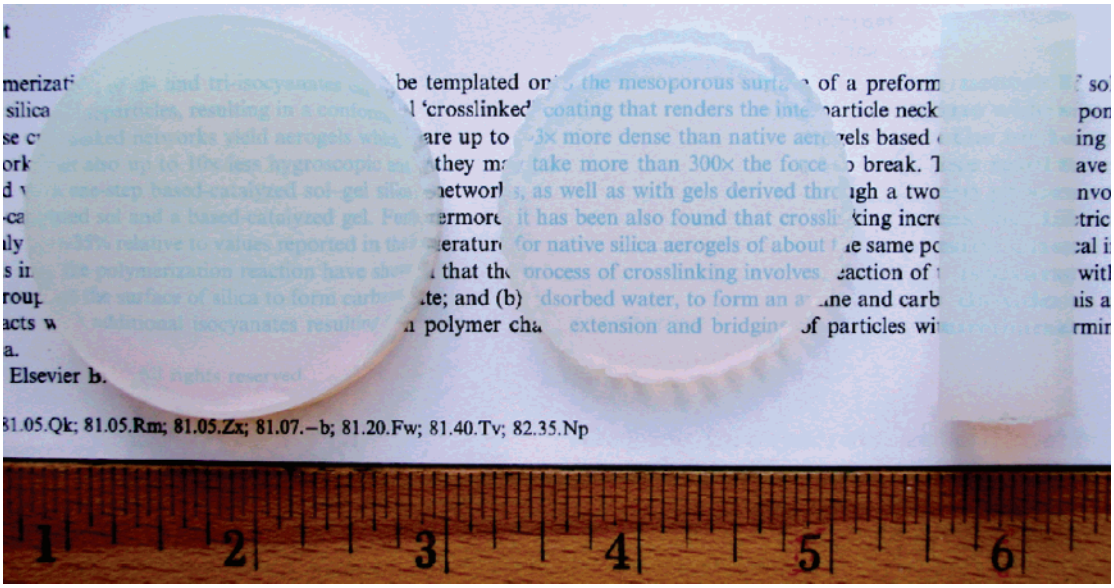

Figure 2. Typical isocyanate cross-linked, amine-modified silica aerogels with density ∼0.48 g cm^{-3}. The cylinder on the right is similar to those used for compressive testing (see Figure 9).

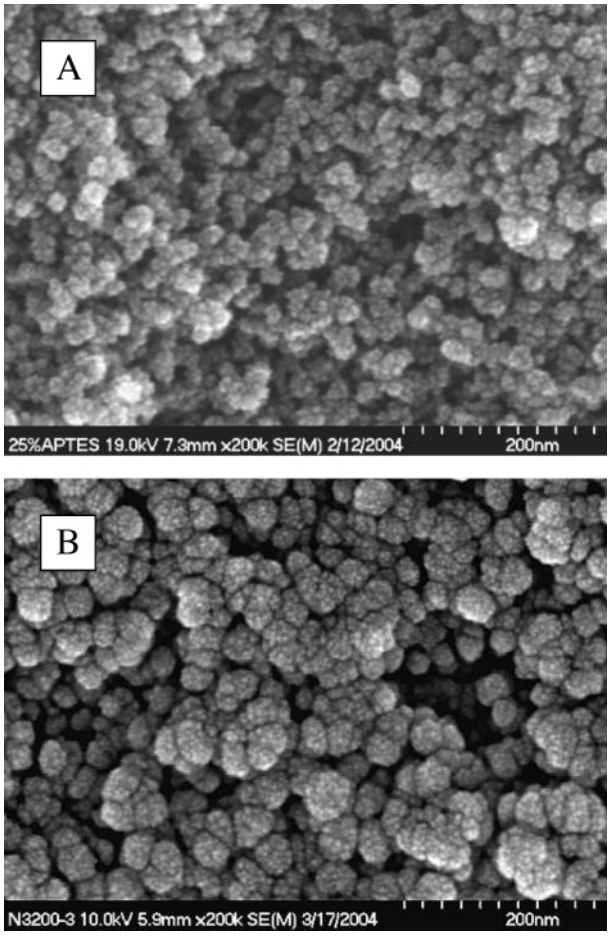

Figure 3. Scanning electron micrographs of (A) a native (non-cross-linked) amine-modified silica aerogel with density ∼0.19 g cm^{-3} and (B) a Desmodur N3200 isocyanate cross-linked amine-modified silica aerogel with density ∼0.48 g cm^{-3}.

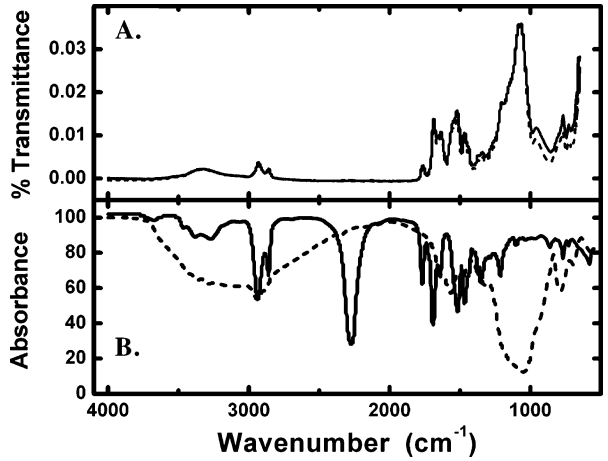

Figure 4. (A) Attenuated total reflectance infrared (ATR-IR) data at the center (—) and the perimeter (---) of a disk cut from a cross-linked aerogel monolith (∼1.6 cm diameter, $\rho \sim 0.48$ g cm^{-3}). (B) Infrared (IR) spectra of Desmodur N3200 diisocyanate oligomer (—, neat) and of a native amine-modified silica aerogel (---, in KBr).

cross-linking. That modification was motivated by the fact that aerogels cross-linked in the isocyanate bath show (by ATR-IR) an up to 30% higher concentration of polymer near the perimeter of ∼0.9 cm diameter monoliths relative to their center.[5d] By comparison, ∼1.6 cm diameter monoliths prepared by the method outlined here show no detectable variation in the polymer between the perimeter and the center of the monoliths (Figure 4A).

By further comparison of the infrared spectrum of cross-linked aerogels (Figure 4A) with the spectrum of the monomer, it is concluded that all the isocyanate has reacted, while the diazetidinedione group of the monomer (1767 cm^{-1}) has survived the cross-linking process. Infrared spectroscopy, however, is rather inconclusive regarding the nature of the polymer as the urea absorbance at 1696 cm^{-1} overlaps with the strong carbamate absorbance at 1690 cm^{-1}, which is already present in the monomer. The carbonyl region of the ^{13}C NMR spectrum (Figure 5B) is also inconclusive, as the diazetidinedione resonance at ∼155 ppm, the carbamate resonance of the monomer at ∼157 ppm, and the urea resonance at ∼160 ppm partially overlap, resulting in a broad absorption.[5d] Nevertheless, a comparison of the ^{13}C NMR spectra of (a) a Desmodur N3200 cross-linked non-APTES-modified aerogel from our previous studies (Figure

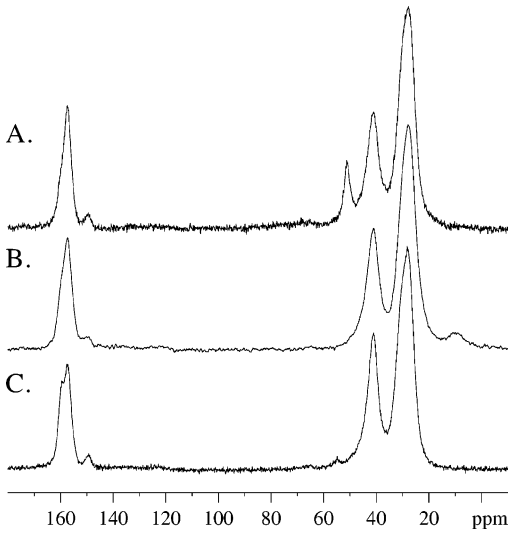

Figure 5. ^{13}C NMR spectra of (A) a Desmodur N3200 cross-linked silica aerogel monolith ($\rho \sim 0.45$ g cm^{-3}) *not* modified with amines, (B) a cross-linked amine-modified silica aerogel sample ($\rho \sim 0.48$ g cm^{-3}), and (C) polyurea produced by exposing Desmodur N3200 to ambient moisture for 10 days.

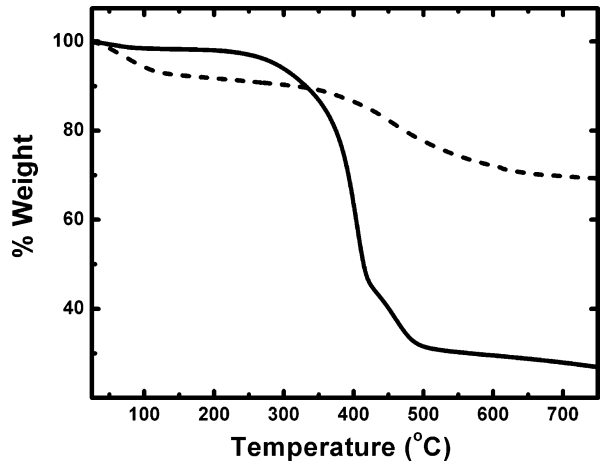

Figure 6. Thermogravimetric analysis (TGA) data under nitrogen of a Desmodur N3200 cross-linked amine-modified silica aerogel sample ($\rho \sim 0.48$ g cm^{-3}, —) in comparison to a native amine-modified aerogel ($\rho \sim 0.19$ g cm^{-3}, ---). (Heating rate: 10 °C/min).

5A), (b) a similarly cross-linked APTES-modified aerogel from the present study (Figure 5B), and (c) polyurea produced by exposing Desmodur N3200 to ambient moisture for a few days (Figure 5C) shows that the resonance at 51 ppm (attributed to carbamate formation with surface silanols) is missing from the spectrum of the cross-linked APTES-modified aerogel, which in turn is identical to the spectrum of Desmodur N3200-derived polyurea. These data suggest that with APTES-modified gels isocyanate reacts preferentially with the surface amines, forming urea, rather than with residual silanols (forming carbamate). Thus, the proposed structure of the polymeric cross-linker is

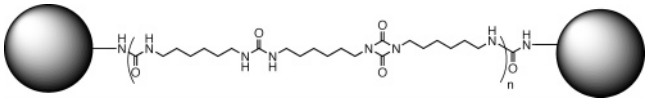

Comparative thermogravimetric analysis (Figure 6) shows that native APTES-modified aerogels experience a significantly higher mass loss below 200 °C compared to their cross-linked counterparts (~10% w/w versus 3−4%, respectively), which is attributed to adsorbed water. On the other hand, the amount of the organic material lost from native aerogels at higher temperatures (>400 °C) is attributed mainly to the propyl groups from APTES and accounts for ~20% w/w of the total mass of the aerogels. Meanwhile, cross-linked aerogels lose 75% of their weight at high temperatures (>300 °C), which, after correction for adsorbed water (~4% w/w) and for the organic matter coming from APTES (scaled back to 13% w/w), indicates that polyurea comprises ~58% w/w of the composite. This figure agrees well with the increase in bulk density by cross-linking (0.478 g cm^{-3} after cross-linking versus 0.190 g cm^{-3} before cross-linking), which corresponds to ~60% w/w of polymer. Further supporting evidence for the composition of cross-linked aerogels comes from skeletal density considerations: the skeletal density of our APTES-modified native silica aerogels is 1.74 ± 0.03 g cm^{-3}. The bulk density of Desmodur N3200-derived polyurea (for sample preparation see discussion of NMR above) is 1.14591 g cm^{-3}. Therefore, the calculated skeletal density of a cross-linked aerogel consisting of 58% w/w polyurea, 4% water, and a balance of APTES-modified silica is expected to be 1.37 g cm^{-3}. The skeletal density of cross-linked aerogels of this study with density ~0.48 g cm^{-3} was found equal to 1.36 ± 0.01 g cm^{-3}. Having developed a sound understanding of the composition of the composite and based on (a) the molecular weight of the main monomer repeat unit (452), (b) the surface area of the cross-linked samples (261 m^2 g^{-1}), and (c) the assumed value of 10^{-10} mol cm^{-2} for monolayer coverage, it is calculated that an average cross-linking tether consists of $n = 5.1$ monomer units.

All data seem to indicate that the cross-linked aerogels of this study retain a fairly open pore structure. Indeed, based on bulk (ρ_b) vs skeletal (ρ_s) density measurements of native APTES-modified silica aerogels, and of our cross-linked samples, it is calculated (eq 1) that our native aerogels with $\rho_b \sim 0.19$ g cm^{-3} are 89% porous, while our cross-linked

$$\text{porosity} = \frac{1/\rho_b - 1/\rho_s}{1/\rho_b} \times 100\% \qquad (1)$$

samples with $\rho_b \sim 0.48$ g cm^{-3} are 65% porous. Such a relatively high level of porosity should retain the principal desirable properties of typical aerogels, namely, a low value for its thermal conductivity, k.[11] The latter was calculated from the thermal diffusivity (α) of a suitable sample (see Experimental Section) using eq 2, where C_p is the

$$k = C_p \cdot \alpha \cdot \rho_b \qquad (2)$$

heat capacity of the material. The thermal diffusivity was measured using a flash method (see Experimental Section),[12] where the sample is heated from one side and we observe the temperature rise on the other. Typical data are shown in Figure 7; the detector voltage, V, is proportional to the

(11) Smith, D. M.; Maskara, A.; Boes, U. *J. Non-Cryst. Solids* **1998**, *225*, 254−259.
(12) Parker, W. J.; Jenkins, J. J.; Abbott, G. L.; Butler, C. P. *J. Appl. Phys.* **1961**, *32*, 1679−1684.

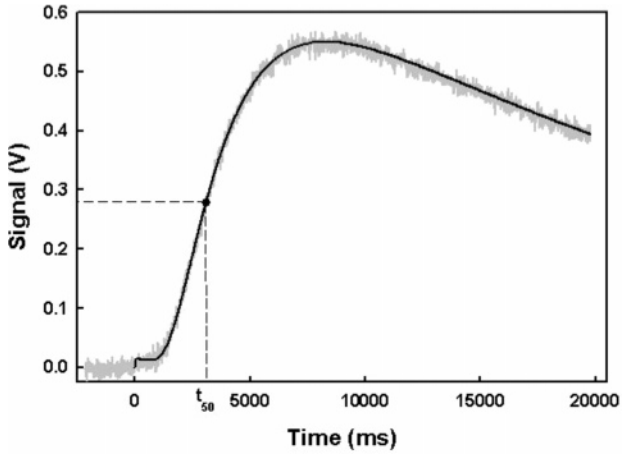

Figure 7. Temperature rise curve of the back face of a Desmodur N3200 cross-linked silica aerogel sample ($8 \times 8 \times 1.386$ mm, $\rho_b = 0.451$ g cm^{-3}) coated with gold and carbon, following a heat pulse incident on the front face. Dashed reference lines indicate t_{50}, that is, the time it takes for the detector voltage to reach $V/V_{max} = 0.5$ (note: voltage ~ temperature).

temperature. The data analysis software approximates a solution to the heat transfer equation by assuming that the sample is opaque to radiative heat transfer. Coating the samples on both sides with gold and carbon validates this assumption by ensuring complete absorption of the heat pulse, effectively eliminating radiative pathways and pulse "bleed through" in the data,[13] and thus a "radiative" spike at the beginning of the rising part of the curve of Figure 7 is not observed. Mathematical models of the temperature rise profile of Figure 7 are generated within the software using an initial value for thermal diffusivity, estimated by the time it takes for the detector voltage to reach $V/V_{max} = 0.5$ (marked as t_{50} time). Subsequently, a least-squares fit is iteratively performed in a defined time range (10 times t_{50}), and a value for thermal diffusivity, α, is obtained. It is noted that $10 \times t_{50}$ has been found to be a suitable measure of the initial cooling event after the sample experiences maximum heating from the heat pulse. Thus, for example, the thermal diffusivity of a polyurea cross-linked APTES-modified aerogel sample 1.386 mm thick ($\rho = 0.451$ g cm^{-3}) was measured at 0.090 ± 0.002 mm^2 s^{-1}. Since that sample consists of ~60% polyurea (expected heat capacity similar to that of polyurethane: ~0.8−1.6 J g^{-1} K^{-1}) and the remaining ~40% amorphous silica (heat capacity ~0.72 J g^{-1} K^{-1}),[14] the heat capacity is calculated as the weighted average at ~1.0 J g^{-1} K^{-1}. These values of density, heat capacity, and thermal diffusivity are introduced in eq 2 and yield a thermal conductivity of 0.041 ± 0.001 W m^{-1} K^{-1},[15] which is in the range of glass wool (0.040 W m^{-1} K^{-1}), Styrofoam (0.030 W m^{-1} K^{-1}), and polyurethane foam (0.026 W m^{-1} K^{-1}).[16]

3.2. Mechanical Testing. Since mechanical strength is the most noticeable property enhancement of cross-linked aerogels, special attention is given to their mechanical properties. The temperature range for testing was decided through initial

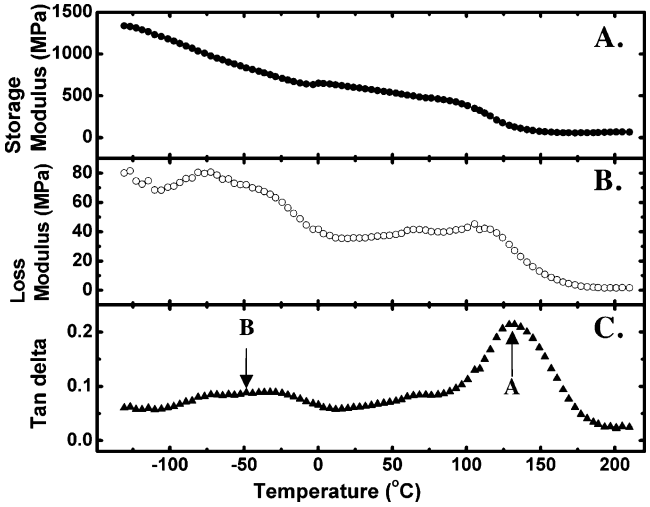

Figure 8. Dynamic mechanical analysis (DMA) on a Desmodur N3200 cross-linked APTES-modified silica aerogel ($\rho \sim 0.67$ g cm^{-3}). Data were collected in a three-point bending mode with loads applied sinusoidaly at 1 Hz. (A) Variation of storage modulus with temperature; (B) Variation of the loss modulus with temperature. (C) Variation of tan(δ) with temperature.

profiling of the mechanical behavior by Dynamic Mechanical Analysis (DMA). The compressive strength of this class of materials is reported for the first time.

3.2.a. Dynamic Mechanical Analysis. Complex modulus data (with storage modulus as the real part and loss modulus as the imaginary part) were collected in a three-point bending mode in the temperature range of −132 to 210 °C. Since the sample dimensions change with temperature (at elevated temperatures samples tend to shrink somewhat), the computation of the complex modulus employed values of nominal stress and nominal strain so that the complex modulus reported should be considered as a "nominal" complex modulus rather than the "true" complex modulus at each temperature. Figure 8A shows the storage modulus as a function of temperature. From these data we determined that the modulus at room temperature is 611 MPa. Since our samples have a low mass density, typically a third (or less) of the density of engineering polymers such as polyethylene and polypropylene,[17] it is concluded that amine-modified, isocyanate cross-linked silica aerogels have a comparable or higher specific modulus than engineering polymers. In general, the storage modulus (Figure 8A) decreases with temperature: at −132 °C, the storage modulus is 1.35 GPa, while at 100 °C it has been reduced to 328 MPa. Around 130 °C, the storage modulus decreases with a steeper rate, thereby indicating an α-glass transition. Above 130 °C, the storage modulus shows a slight increase, but at the end (210 °C) it has been reduced to only 66.5 MPa, i.e., about 5% of its value at −132 °C. Finally, at ca. −50 °C, the storage modulus shows a second steep reduction, indicating a possible second glass transition. Figure 8B shows the loss modulus, and Figure 8C presents the tangent of the out-of-phase angle (δ) in radians, between sinusoidal load and sinusoidal displacement. In a typical viscoelastic material, the sinusoidal load is ahead of sinusoidal displacement by a phase angle between 0 and $\pi/2$.[18] The loss modulus

(13) Lee, D.; Stevens, P. C.; Zeng, S. Q.; Hunt, A. J. *J. Non-Cryst. Solids* **1995**, *186*, 285−290.
(14) Anderson, S.; Dzhavadov, L. *J. Phys.: Condens. Matter* **1992**, *4*, 6209−6216.
(15) Corresponding to an *R*-value equal to 3.5/in.
(16) Lide, D. R. *CRC Handbook of Chemistry and Physics 84th Edition*; CRC Press: Boca Raton, FL, 2003; pp 12/226−12/227.
(17) Menard, K. P. *Dynamic Mechanical Analysis*; CRC Press: Boca Raton, FL, 1999.

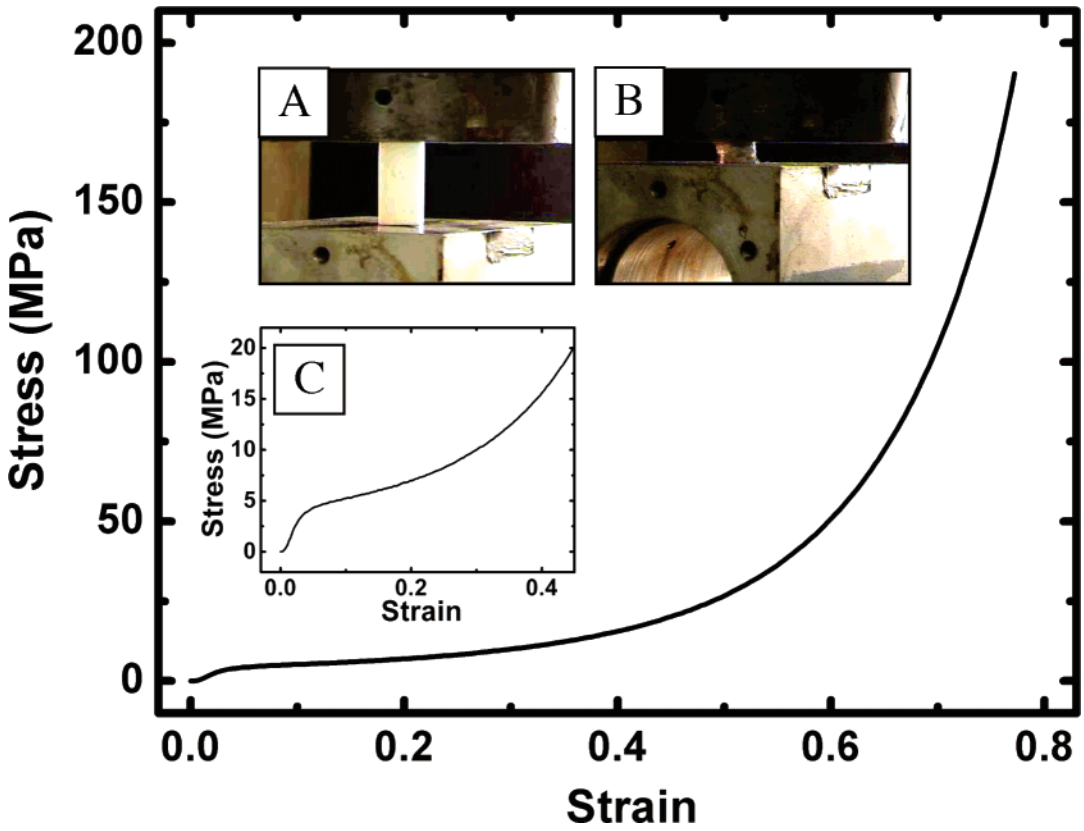

Figure 9. Mechanical compression testing of a Desmodur N3200 cross-linked APTES-modified silica aerogel cylinder ~ 0.5 in. diameter, ~1 in. long with $\rho \sim 0.48$ g cm^{-3}. *Inset A*: The setup before testing. *Inset B*: The setup at the point of collapse. *Inset C*: Expanded low-strain range. (Strain rate = 0.0035 s^{-1}.) (The sample illumination was from the front, and the translucency shown in Figure 2 is not evident.)

(Figure 8B) was computed in terms of storage modulus multiplied by the loss tangent, tan(δ). From Figure 8C, we note that there is a major peak in tan(δ) around 130 °C, labeled as "A." The peak indicates that our material undergoes softening (a high-to-low viscosity transition) around that temperature. These data taken together with the rapid decrease in the storage modulus around the same temperature confirm that the major glass transition temperature (α-transition) is at 130 °C.[17] The second peak in Figure 8C at around −50 °C, labeled as B, indicates a secondary glass transition (β-transition), in support of the storage modulus data (Figure 8A). Overall, our samples will show the strongest time- and rate-dependent behavior around 130 °C, but they will show pronounced time- and rate-dependent behavior also at around −50 °C. Clearly, for structural applications, amine-modified, isocyanate cross-linked aerogels must be used well below 130 °C, and in fact these materials are expected to demonstrate their best mechanical behavior at room temperature and below. Thus, further mechanical testing was concentrated between room and cryogenic temperatures.

3.2.b. Compression Testing. Figure 9 shows typical stress−strain data for isocyanate cross-linked APTES-modified silica aerogel specimens under compressive loading at room temperature. Inset A shows the experimental setup at the beginning of the test, inset B shows the sample at failure, and inset C shows a magnification of the lower strain range of the stress−strain curve. (An actual movie (Movie S.1) showing a sample undergoing compression testing as well as high-speed photography that captures the crack initiation and failure under compression are given in Supporting Information.) Data on compressive yield strength, compressive stress at ultimate failure, and Young's modulus for individual samples, as well as the average values with their standard deviations, are summarized in Table 1. The compressive yield strength is the 0.2% (compressive strain) offset yield strength determined from stress−strain curves similar to those of Figure 9 following the ASTM D695-02a standard. The ultimate compressive strength data of native amine-modified silica aerogels are given in Table 2 for comparison. It is noted that the stress−strain relationships for the native sample of Table 2 are nearly linear up to failure so that it is sufficient to quote only their ultimate compressive strength. It is observed that in compression, cross-linked aerogels of this study are linearly elastic under small compressive strains (<4%) and then exhibit yield (until

Table 1. Summary of Compressive Strength Data of Isocyanate Cross-linked Amine-Modified Silica Aerogels at a Strain Rate of 0.0035 s^{-1}

sample number	density (g·cm^{-3})	compressive yield strength (MPa)	compressive stress at final failure (MPa)	failure strain (%)	Young's modulus (MPa)
1	0.48	4.19	190.33	77.22	122.85
2	0.47	4.25	222.08	77.04	119.58
3	0.48	3.88	168.55	77.2	126.27
4	0.48	4.47	173.72	76.1	135.27
5	0.48	4.50	173.20	78.35	138.94
average	0.478 ± 0.004	4.26 ± 0.25	186 ± 22	77.2 ± 0.8	129 ± 8

(18) Ward, I. M.; Hadley, D. W. *An Introduction to the Mechanical Properties of Solid Polymers*; Wiley: New York, 1997.

Table 2. Summary of Compressive Strength Data of Amine-Modified Native Silica Aerogels at a Strain Rate of 0.0035 s^{-1}

sample number	density ($g \cdot cm^{-3}$)	ultimate compressive strength (MPa)	failure strain (%)	Young's modulus (MPa)
1	0.18	4.00	5.31	96.69
2	0.20	4.09_5	6.00	86.94
average	0.19 ± 0.01	4.05 ± 0.05	5.66 ± 0.49	92 ± 7

~40% compressive strain), followed by densification and inelastic hardening; they ultimately fail at ~77% compressive strain, yielding an ultimate compressive strength of 186 ± 22 MPa. The average yield stress defined at the beginning of densification is 4.0 ± 0.2 MPa and occurs at ~4% strain. Interestingly, samples did not exhibit significant lateral dilatation (the Poisson ratio is only 0.18) and did not buckle in compression. At failure, the outer layer of all samples shattered and fell away, while all remaining cores (e.g., Figure 9, inset B) have the same height, indicating that failure is due ultimately to lateral tensile stresses even though the applied load is compressive. Both the strain at failure and the ultimate compressive strength are much higher than those of native (non-cross-linked) aerogels due to the underlying cross-linked silica framework. Native aerogels fail at about 5.7 ± 0.5% strain, exhibiting an ultimate compressive strength of only 4.1 ± 0.1 MPa (Table 2). By comparison, cross-linking has increased failure strain by a factor of 13.5 and increased compressive strength by a factor of 45. Attempts to prepare monoliths of native APTES-modified silica aerogels of similar density as our cross-linked samples failed because of extensive cracking developed during washings, presumably due to high internal stresses. Nevertheless, assuming a power law dependence of the yield strength (σ_s) on density (ρ), $\sigma_s \sim \rho^{\alpha}$,[19] it is calculated from the strength data of Tables 1 and 2 that $\alpha = 4.14$. The literature value for α measured from the failure strength (three-point bending test) of native silica aerogels is 2.6 ± 0.2.[19] Therefore, consistent with our previous semiquantitative results,[5d] increasing density by adding silica is not as effective a method to increase strength as by adding a conformal polymer coating on the skeletal framework, which, presumably, renders interparticle necks wider.

For comparison with other materials, the specific compressive yield strength of our cross-linked aerogels is calculated at 8900 N m kg^{-1} and the specific compressive stress at ultimate failure at 3.89×10^5 N m kg^{-1}. While the specific compressive yield strength of our samples is much lower than the values of typical structural materials (representative examples are given in Supporting Information), the specific compressive stress at ultimate failure is reasonably high, on the same order of magnitude as some engineering materials such as poly(methyl methacrylate) (PMMA)[20] and Kevlar-49 epoxy.[21] The relatively high specific compressive stress at ultimate failure in combination with its low thermal conductivity would render polyurea cross-linked aerogels attractive as multifunctional materials for applications where catastrophic failure could not be tolerated, as for example in cryogenic tanks.

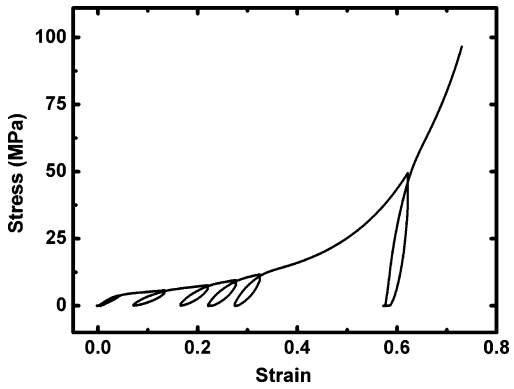

Figure 10. Load−unload testing of a Desmodur N3200 cross-linked APTES-modified silica aerogel cylinder ~ 0.5 in. diameter, ~1 in. long ($\rho \sim 0.48$ g cm^{-3}).

Young's modulus in compression was evaluated from the slope of the initial linear portion (at <4% strain) of the stress−strain curve. The Young's modulus of the cross-linked aerogel is 129 ± 8 versus 92 ± 7 MPa of the native silica framework. But the elastic part of the stress−strain curve has other similar characteristics with the stress−strain curve of the underlying native silica framework as well: it extends up to ~4.26 MPa and ~4% strain, while the native silica framework fails at 4.1 ± 0.1 MPa and 5.7 ± 0.9% strain. These data seem to suggest that at small strains the mechanical behavior of the composite material, at the specific silica-to-polymer ratio, is shaped by the stiffer silica framework, while at higher strains, the behavior of the material under compression is controlled by the conformal polymer coating.[22] That realization should be reflected in the recovery (springback) behavior of the material during loading−unloading cycles along the stress−strain curve. Indeed, a typical cylindrical sample was loaded and unloaded six times, first in the elastic region where deformation is completely recovered (Figure 10). Then it was unloaded and reloaded in the plastic region where a hysteresis loop was always observed, presumably due to energy loss because of slipping of polymer chains.[20] It is further noted that the percent strain recovery becomes progressively lower at higher strains, while in the inelastic hardened range (~60% strain) there is practically no strain recovery. The changes in the morphology of the material under inelastic compression were evaluated by SEM (Figure 11) and porosity/surface area analysis (Table 3). For this, samples were loaded up to a predetermined strain and subsequently the load was removed and the samples were analyzed. Curiously, under SEM, the material does not show any noticeable difference from its original state up to at least 45% strain (only part of which is recovered by removing the load, see Figure 10). Surface area analysis, however, shows unambiguously that as the degree of plastic deforma-

(19) (a) Woignier, T.; Reynes, J.; Hafidi Alaoui, A.; Beurroies, I.; Phalippou, J. *J. Non-Cryst. Solids* **1998**, *241*, 45−52. (b) Woignier, T.; Phalippou, J. *Rev. Phys. Appl.* **1989**, *24*, 179−184.

(20) Ferry, J. D. *Viscoelastic Properties of Polymers, Third Edition*; Wiley: New York, 1980.

(21) American Society for Metals. *ASM Engineering Materials Handbook, Composites, Volume 1*: ASM International: Materials Park, OH, 1998; p 178, Table 2.

(22) By the same token, the somewhat higher modulus of cross-linked aerogels relative to their native counterparts (129 versus 92 MPa, respectively) is attributed to the larger diameter of particles in contact, imposing larger restrictions to bending.

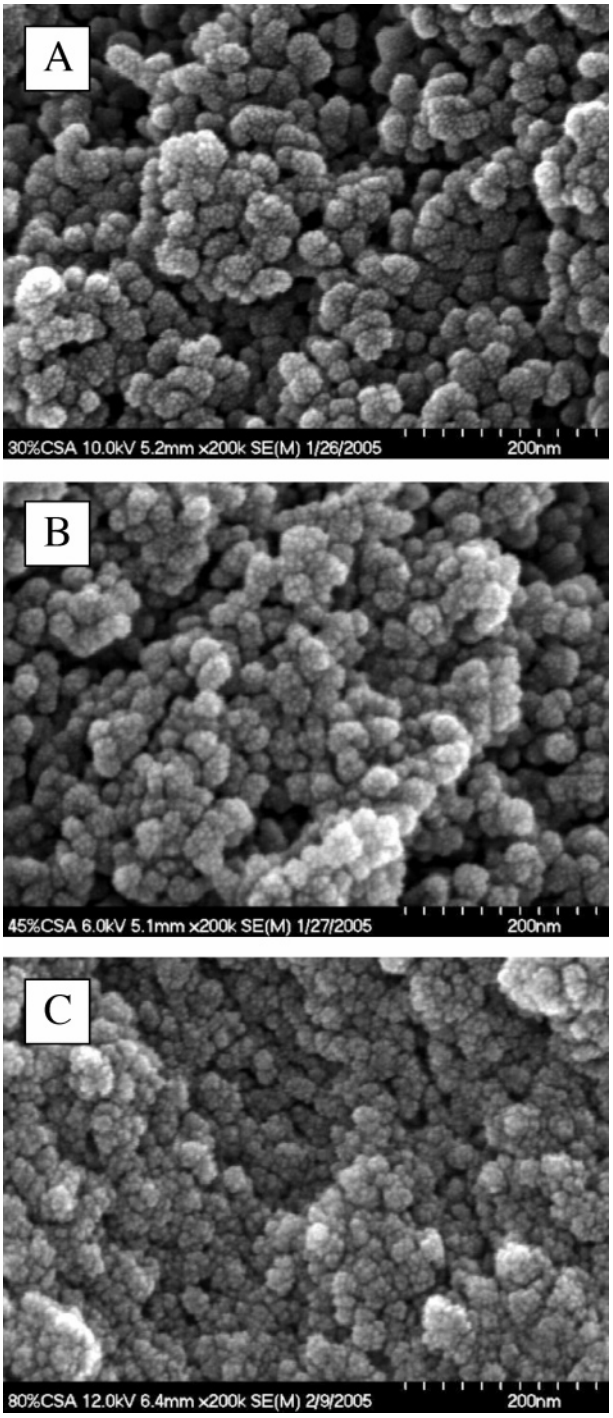

Figure 11. SEM images of the morphological changes after compression in Desmodur N3200 cross-linked APTES-modified silica aerogel cylinders ~0.5 in. diameter, ~1 in. long ($\rho \sim 0.48$ g cm^{-3}). (A) At 30% strain; (B) At 45% strain; (C) At 77% strain.

Table 3. Surface Area Analysis along Compression of Isocyanate Cross-linked Amine-Modified Aerogels ($\rho = 0.48$ g cm^{-3})

strain (%)	BET surface area (m^2 g^{-1})	average pore diameter (nm)
0	261	9.7
30	197	15.2
45	152	169
77	6	*a*

[a] Low *c*-value (5.22) and isotherms not well-defined.

tion increases, the surface area decreases and the average pore diameter increases, consistent with loss of mesoporosity as particles are squeezed closer to one another permanently. Ultimately, at failure (77% strain) SEM shows clear signs of collapse, i.e., a nearly total loss of porosity, also supported by surface area analysis.

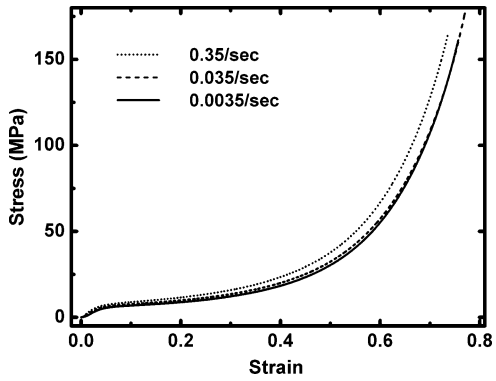

Figure 12. Effect of the strain rate on the behavior under compression of Desmodur N3200 cross-linked APTES-modified silica aerogel cylinders ~0.5 in. diameter, ~1 in. long ($\rho \sim 0.48$ g cm^{-3}).

Overall, with the elastic limit in compression at room temperature of isocyanate cross-linked aerogels being approximately 4.26 MPa, and with the compressive failure strain also high (~77%), the resilience (energy absorption), indicated by the area enclosed by the stress−strain curve is also very high, making these materials suitable candidates for energy absorption in structures subjected to impact/penetration loadings.

Finally, the effects of the strain rate and temperature on the ultimate compressive strength were both evaluated. Figure 12 shows stress−strain curves at three compressive strain rates, 0.0035, 0.035, and 0.35 s^{-1}. Although the Young's modulus increases with an increase in strain rate (128, 160, and 205 MPa at strain rates of 0.0035, 0.035, and 0.35 s^{-1}, respectively), as the strain rate was varied by a factor of 100, the overall stress−strain curves did not change significantly, indicating that increased strain rate does not have a deleterious effect on the energy-absorption behavior of cross-linked aerogels under compression within the range of strain rates tested. If this result is considered together with the resilience of the material, it points toward ballistic applications and suggests further experimentation at very high strain rates via the split Hopkinson bar test, where strain rates up to 10^4 s^{-1} can be applied.

Figure 13 shows the stress−strain curves for cross-linked aerogel samples in compression testing at various temperatures. Mechanical response is essentially invariant of the temperature in the range between 21 and −55 °C. However, the material stiffens significantly (the elastic modulus increases to ~450 MPa) and suffers premature compressive failure at cryogenic temperatures (e.g., −196 °C).

3.2.c. Flexural Testing. Figure 14 shows the stress−strain curves obtained through three-point bending tests conducted with samples with mass density of 0.48 g cm^{-3} at room temperature. Table 4 summarizes the results and includes the flexural modulus, which provides an estimate of the tensile modulus for a material. (Movie S.2 showing a sample undergoing flexural testing, the actual load deflection data, and the data analysis method for deriving the stress−strain curves of Figure 14 are given as Supporting Information.)

Table 4. Results for Three-Point Bending on Isocyanate Cross-linked Amine-Modified Silica Aerogels at a Strain Rate of 0.0011 s^{-1}

sample	temperature	density ($g \cdot cm^{-3}$)	failure load (lbs/kg)	square dimm. (mm)	failure disp. (mm)	flexural modulus (MPa)	flexural strength (MPa)	flexural strength (psi)
1	21 °C	0.48	48.24/21.93	13.9	1.90	181	11.99	1740
2	21 °C	0.48	42.14/19.15	13.9	1.77	160	10.48	1520
3	21 °C	0.48	33.4/15.18	13.7	1.58	160	8.67	1260
average of 1−3 (21 °C)						167	10.38	1500
4	−196 °C	0.48	45.27/20.6	13.5	0.855	360	11.50	1670
5	−196 °C	0.48	39.1/17.8	13.8	0.558	517	10.6	1540
average of 4−5 (−196 °C)						438.5	11.05	1600
6	21 °C	0.76	88.1/40.0	9.5	1.88	723	50.59	7332
7	21 °C	0.78	82.3/37.4	9.5	1.62	774	54.16	7850
average of 6−7 (21 °C)		0.77	85.2/38.7	9.5	1.75	748	52.38	7591

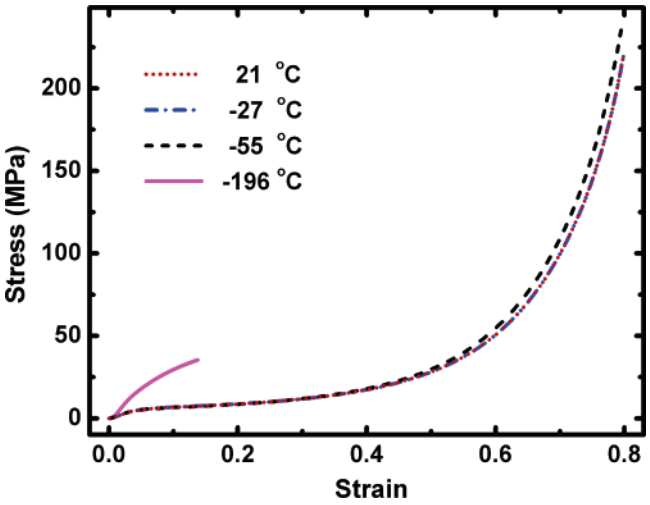

Figure 13. Effect of temperature on the behavior under compression of Desmodur N3200 cross-linked APTES-modified silica aerogel cylinders ~0.5 in. diameter, ~1 in. long ($\rho \sim 0.48$ g cm^{-3}).

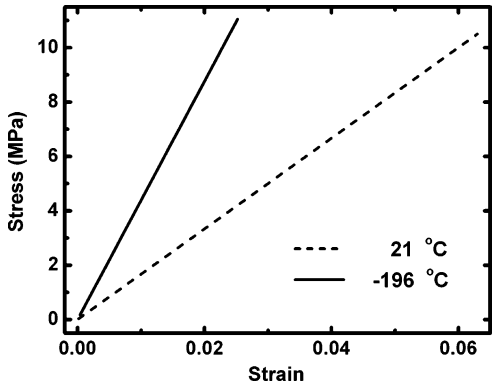

Figure 14. Three-point bending tests on Desmodur N3200 cross-linked APTES-modified silica aerogel rectangular samples with nominal dimensions of 11 × 11 × 50 mm ($\rho \sim 0.48$ g cm^{-3}).

The stress−strain curves of Figure 14 are linear with an average flexural modulus of 167 MPa at room temperature. At cryogenic temperatures (−196 °C) the lower bound of the flexural modulus is 360 MPa, almost double the room-temperature value. The flexural strength (~11 MPa) shows also a slight increase, thereby confirming the capability of our samples to sustain bending loads at cryogenic temperatures. By the same token, however, since our material exhibits a bimodal behavior, i.e., its elastic modulus in compression is considerably lower than the modulus from bending tests (compare results in Tables 1 and 4), additional tensile testing must be performed to obtain the actual Young's modulus in tension.

Table 4 also includes flexural modulus and strength data for two samples with higher densities: 0.76 and 0.78 g cm^{-3}, respectively. The flexural moduli of those samples are 723 and 774 MPa. These values are much higher than the average flexural modulus of samples with a mass density of 0.48 g cm^{-3} (167 MPa). If we assume a power law relationship between the modulus and the mass density ($E \sim \rho^{\beta}$), we determine that $\beta = 3.17$ at room temperature. It is noted that this scaling exponent is not necessarily equal to the scaling exponent between native and cross-linked aerogels ($\alpha = 4.14$, see section 3.2.b). The difference between the two exponents underlines the fact that adding polymer to the silica skeletal framework is a more effective method to increase strength than by adding silica.

Finally, it is also reminded that the storage modulus at room temperature derived from the temperature sweep DMA tests is 611 MPa, i.e., much higher than the flexural modulus of 167 MPa at room temperature from the three-point bending test, even though both tests are performed in the same flexure mode. It is suggested that the following factors could contribute to the higher value in modulus from temperature sweep DMA tests: (1) DMA samples had an average density of ~0.67 g cm^{-3}, which is higher than the density (0.48 g cm^{-3}) of the samples used in three-point bending. Since $E \sim \rho^{3.17}$, and the flexural modulus for samples with mass density ~0.48 g cm^{-3} was determined to be 167 MPa, the scaling relation yields a calculated flexural modulus of 480 MPa for samples with mass density of 0.67 g cm^{-3}, which is closer to the DMA value of 611 MPa; (2) DMA tests were conducted at a flexural frequency of 1 Hz, corresponding to a strain rate of approximately 1 s^{-1}, much higher than the strain rate (~0.0011 s^{-1}) used in three-point bending test; and (3) in temperature sweep DMA tests, the starting point for the temperature sweep was −132 °C, and therefore the temperature history experienced by the DMA specimen at room temperature was very different from that of the three-point bend test at room temperature.

4. Conclusions

Amine-modified aerogels prepared by co-gelation of TMOS with APTES were cross-linked with a polyurea derived from Desmodur N3200 diisocyanate and characterized chemically, physically, and mechanically. From DMA testing it was concluded that the α- and β-transition temperatures are at 130 °C and at −50 °C, respectively. At room temperature the new material is both stiff and strong

in terms of properties per unit density: uniaxial compression tests indicate an average Young's modulus of 129 MPa, leading to a specific Young's modulus of 2.7×10^5 N m kg^{-1}, and an average compressive stress at ultimate failure of 186 MPa, yielding a value of 3.89×10^5 N m kg^{-1}. All compressive specimens failed due to lateral tension. Compression tests at lower temperature did not result in a significant change in the properties down to −55 °C, although further testing at cryogenic temperatures is necessary before this trend can be fully confirmed. The average flexural modulus was determined to be 167 MPa at room temperature. At cryogenic temperature (−196 °C) the flexural modulus is almost doubled, and the flexural strength (∼11 MPa) shows a slight increase, thereby confirming the capability of polyurea-cross-linked, amine-modified aerogels to sustain bending loads at cryogenic temperatures. Overall, with a thermal conductivity at ∼0.041 W m^{-1} K^{-1} and an ultimate specific compressive strength similar to that of some engineering materials such as PMMA and Kevlar-49 epoxy, our results indicate that these materials can be used for the dual purpose of a thermal insulator/structural component with applications wherever saving weight is critical.

Acknowledgment. Financial support from NASA Glenn Research Center (NNC04GB54G) is gratefully acknowledged. We thank Dr. Brian Grady of the University of Oklahoma for the DMA tests, Dr. Mary Ann Meador of NASA GRC for her assistance with NMR, Mr. Robert Campbell of Netzsch Instruments, Inc. for his help with the thermal conductivity tests, Mrs. Anna Palczer of NASA GRC for the surface analysis, and Mrs. Linda McCorkle of the Ohio Aerospace Institute for SEM. We also thank Bayer Corporation for the generous supply of isocyanates.

Supporting Information Available: Nitrogen adsorption isotherms for native and cross-linked samples; high-speed photography capturing the crack initiation and failure under compression; comparison of specific strength data of isocyanate-cross-linked amine-modified silica aerogels with various materials; load/deflection data from a three-point characterization test, and data analysis; Movie S.1: compression testing; Movie S.2: three-point bending test. This material is available free of charge via the Internet at http://pubs.acs.org.

CM0513841